Implementation of a beam hardening correction method for mono material parts using a linearization technique

Andreas Michael MÜLLER [1], Lorenz BUTZHAMMER [1], Tino HAUSOTTE [1]
[1] Institute of Manufacturing Metrology (FMT), Friedrich-Alexander-Universität Erlangen-Nürnberg (FAU), Erlangen, Germany

Contact e-mail: andreas.mueller@fmt.fau.de

Abstract. Common X-ray sources for industrial computed tomography (CT) exhibit a polychromatic spectrum. While the absorption of radiation by the measurement object is dependent on the X-ray energy, the commonly used reconstruction algorithms assume an absorption coefficient under monochromatic conditions. In the context of industrial CT, the material of a measurement object is oftentimes known, which makes the application of a linearizing beam hardening correction method possible for parts made out of a single material. In this work, we present an efficient setup and data processing pipeline to determine and manage experimental X-ray absorption models for mono material parts. This pipeline estimates the correlation between attenuation and penetration length using a cone shaped specimen and subsequently corrects the grey values of the projections of a measurement object of the same material as the specimen. In contrast to commonly used step wedges, the special specimen makes it possible to sample the absorption curve with a large number of grid points, while using a standard measurement operation mode for the CT system. The correction method makes it possible to measure the tooth flanks of a steel gear wheel, which could otherwise not be measured due to beam hardening artefacts.

Introduction – Beam Hardening and Correction Concepts

The physical interaction of electromagnetic radiation with matter causes the radiation to be attenuated, which is described by the Lambert-Beer law in Eq. (1).

$$I = \int_0^{E_{max}} I_0(E) \cdot e^{-\int_0^l \mu(E,\rho,Z,x)dx} dE \tag{1}$$

The intensity I_0 of the photons is attenuated along their path through all the volume elements of a penetrated object with thickness l dependent on the attenuation coefficient $\mu(E,\rho,Z,x)$, which is dependent on the energy of radiation E as well as on the density ρ and the atomic number Z of the volume elements. X-ray computed tomography (CT) in general assumes a straight-line propagation and an energy-independent absorption coefficient when applying standard reconstruction techniques like the commonly used FDK algorithm [1] for cone-beam CT. The generation of monochromatic X-rays with sufficiently large intensity to be used in industrial computed tomography is currently not possible (except for rare and expensive synchrotron accelerators). Consequently, X-ray tubes are almost exclusively used to generate the radiation required for the imaging by accelerating electrons onto a target. This process generates a wide distribution of polychromatic photons, which are then used in the CT imaging process. The energy dependent attenuation of X-rays during penetration of matter causes an increase of the average photon energy, which is called “beam hardening”. X-rays from an identical source passing the same location within a measurement object from different directions consequently show different energy distributions, which leads to different intensity deviations from an ideal monochromatic absorption curve for the same object location. This causes the occurrence of beam hardening artefacts, which can prevent the correct determination of the surface of the measurement object by examination of the volume data [2].

One commonly used method to suppress the effects of beam hardening is the pre-filtration of all generated X-rays. This causes a smaller energy distribution of used photons during the measurement process at the cost of lower X-ray intensities and thus a worse signal-to-noise ratio of the measurements. In the last decades, a lot of different correction methods have been proposed and implemented by the scientific community, X-ray device manufacturers and software companies. Exemplary classifications can be found in [3–5]. Those methods range from dual-energy imaging [6], over volume data post-processing and projection data adjustments and can vary greatly regarding the available and used information of the measurement setup and can oftentimes be limited to certain use cases [2]. An overview over methods to compensate metal artefacts in general can be found in [7, 8].

This contribution has implemented a version of the commonly known linearization technique, which operates on the assumption that for monochromatic radiation, a linear relation exists in the sense of Eq. (2) between X-ray penetration lengths and observed attenuated intensities, if the measurement object exhibits a homogeneous composition. The concept of the linearization describes the approach to transform a measured polychromatic projection value from its nonlinear absorption curve onto the corresponding mono-energetic projection value representing the same penetration length [2, 9].

$$-\ln\left(\frac{I}{I_0}\right) = \mu x \tag{2}$$

The focus was put on presenting a robust, fast and easily adjustable method to repeatedly perform a pre-defined inspection task of steel gear wheels with known material composition. It will be shown, that the measurement task can be fulfilled by the implementation of the beam hardening correction (BHC) routine into the measurement chain and thus expand the fields of applications of the used CT system to steel parts with minimum additional effort.

1. Measurement Task and Used Measurement Setup

The measurement task was defined as the dimensional characterization of a wire-eroded, straight-toothed steel gear wheel (tooth tip diameter 19 mm, thickness 8 mm, material 16MnCr5) using the industrial cone beam CT Zeiss Metrotom 1500. Goal of the examination was the evaluation of the gear tooth flanks. Because of that, the gear wheel was manually positioned within the measurement volume such that the rotation axis of the gear wheel matched the rotation axis of the rotatory stage. This orientation was chosen to ensure the same measurement uncertainty characteristics for each tooth flank. Nonetheless, this resulted in larger average X-ray penetration lengths compared to an upright orientation of the gear wheel and this also meant, that there were no projections showing the contour of the tooth system. Consequently, the criterion for success was defined as being able to evaluate the geometric properties of all tooth flanks. The measurement settings were chosen as follows: tube voltage 225 kV, tube current 200 µA, nominal X-ray spot size 45 µm, detector gain 16x, detector integration time 1000 ms, geometric magnification approx. 19.6, voxel size approx. 10 µm, number of projections 2000. A projection consists of 2038 x 2046 pixels with a pitch of 200 µm and value range of 16 bit. All subsequently mentioned data processing steps were performed using the corrected projections, which also included a flat field correction (Zeiss Metrotom OS). No additional pre-filtration (besides a filter of 0.6 mm aluminium built into the X-ray tube) was used. The built-in ring artefact reduction method was disabled in order to simplify the following data processing pipeline. The tomographic reconstruction was done using the filtered (Shepp-Logan filter kernel [10]) back projection algorithm provided by Siemens CERA XPlorer 3.0.3 [11]. It was not possible to determine the surface of the measurement object in the areas between the gear teeth from the reconstructed volume using VGStudio Max 3.2.5 (VGS), despite experimenting with numerous different algorithm parameters[1]. We also unsuccessfully tried filtering the volume data before the surface determination with Gaussian filters of various cubic kernel sizes using VGS, as well as filtering each projection before reconstruction with a Gaussian filter (sigma = 5 pixel) using MATLAB. Fig. 1 shows a volume data slice of the reconstructed volume. It is clearly observable, that the areas between neighbouring teeth exhibit incorrect grey values, which is caused by beam hardening as well as X-ray scatter artefacts. The measurement task was set to quantitatively evaluate the geometry of the gear teeth of many gears of the same kind in order to determine impacts caused by wear and tear. Because of that, the subsequently described data processing pipeline was set up in order to correct the beam hardening artefacts, which prevented a robust and stable surface determination of these measurements.

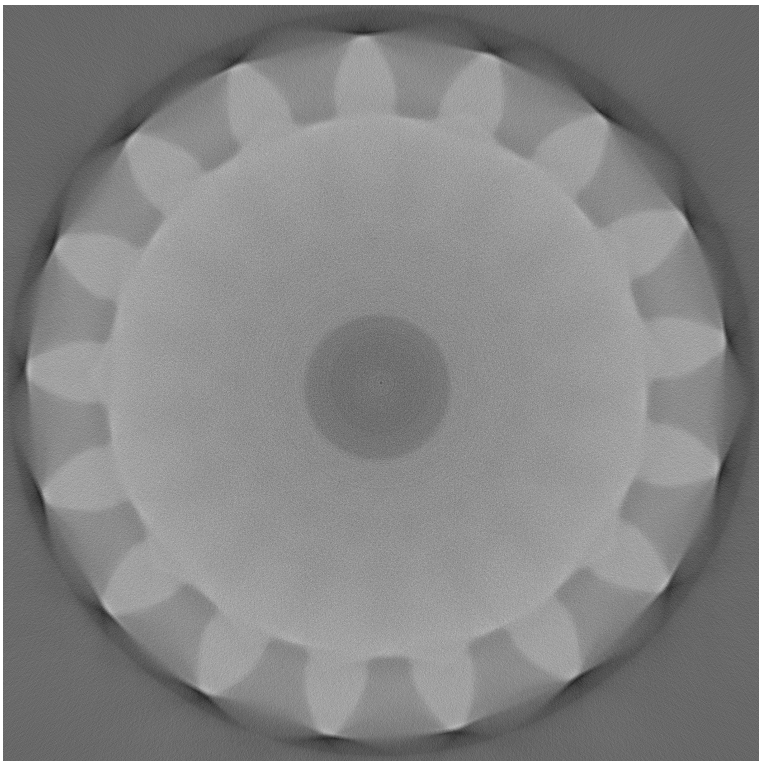

Fig. 1: Visualization of a single volume data slice (z = 630 voxel) of the gear measurement. The beam hardening and X-ray scatter artefacts visible between the gear teeth made it impossible to determine the object surface. The colour maps contain the 16 bit value range resulting after reconstruction.

[1] The presented results in this article are not to be understood as an evaluation of the software performance. Therefore, no detailed descriptions regarding the exact settings applied for the surface determination are given.

2. Data Processing Pipeline for Beam Hardening Correction

In the following chapter, the complete data processing pipeline is described. The main focus was put on implementing a robust, fast and flexible beam hardening correction method for a given CT system and work pieces of known composition. The complete approach is characterized by the following steps:

I. Design and manufacturing of a simple, cone-shaped specimen with homogeneous absorption properties, preferably by using the same material as the measurement object of interest (gear wheel).
II. Performing a complete CT scan using the same CT settings as for the gear wheel measurement.
III. Determining the position and orientation of the measured cone from the determined surface using geometry element regression analysis in VGS.
IV. Extracting the absorption curve by determination of the corresponding cone penetration lengths for each detector pixel in each captured projection.
V. Correction of the projection grey values of the gear wheel measurement using the absorption curve and the associated correction values.
VI. Reconstruction of the corrected projection stack and evaluation of the result.

2.1. Cone shaped Specimen

Usually, a single projection (radiography) of a calibrated normal is used in order to determine the correlation between X-ray penetration length and radiation attenuation [2]. In general, this approach can have several downsides, including:

- Usage of only discrete X-ray penetration lengths,
- Disregarding of the cone beam geometry, which can lead to slightly incorrect X-ray penetration lengths,
- Limited statistical robustness of the measured correlation due to the evaluation of only a small number of observations,
- Necessity of a separate CT system operation program in order to record single projections with adequate image corrections (e.g. flat field correction). These corrections are usually proprietary, meaning corrections equal to those performed within the measurement software cannot be performed.

In order to remedy these possible downsides, a cone-shaped specimen (Fig. 2) was manufactured, which can directly be mounted onto the perforated plate of the rotatory stage. Consequently, the rotation axis of the specimen is then aligned parallel with the rotation axis of CT rotatory stage.

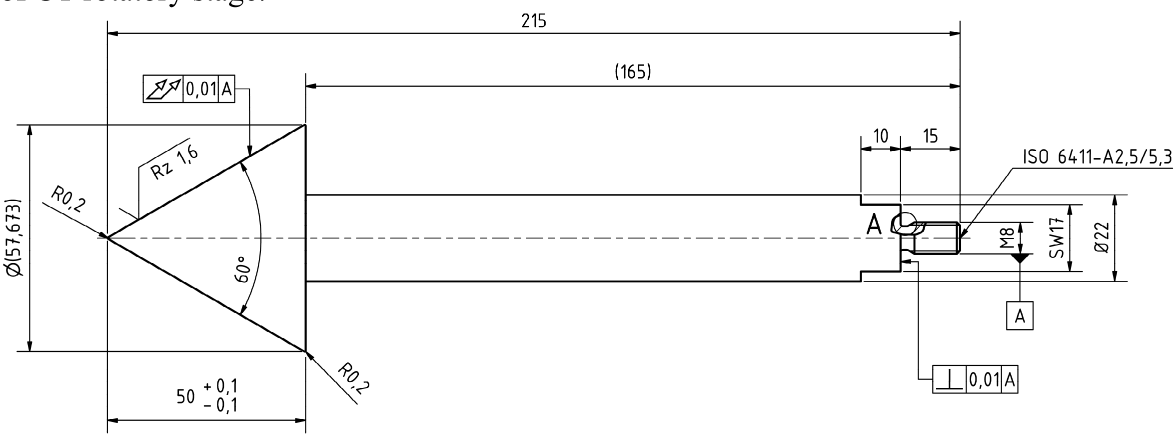

Fig. 2: Technical drawing of the used cone-shaped specimen, which was then mounted in a standing position onto the rotatory stage of the CT, resulting in a parallel alignment of both rotatory axes.

The rotation symmetry of the specimen makes it possible to correctly determine the cone shell surface using locally adaptive CT surface determination routines after the reconstruction, because no object edges are hidden in any projections. This condition is also not affected by the material of the specimen. A correct reconstruction of the cone shell surface would still be possible in case of nearly complete radiation attenuation at the detector. The penetration lengths are not limited to discrete values by the specimen (between the cone tip radius and the maximum cone diameter). This specimen can then be positioned and measured using the same CT settings as for the gear measurement. The evaluation of a large number of projections can then result in a statistically very robust determination of the absorption curve (see subsequent chapter). Additionally, turned parts can be manufactured very accurately and cost efficiently, which makes it feasible to produce additional parts with different material compositions if needed.
For the implementation of the linearization technique it is crucial to use materials with matching absorption properties for both the measurement object and the specimen. In this contribution, we chose the material for the specimen as X5CrNi18-10, because of its availability and its corrosion properties. Despite the different chemical compositions of both alloys (Table 1), the resulting attenuation coefficients are almost identical (Fig. 3).

Table 1: Chemical composition in mass percent of the alloys of the gear wheel (16MnCr5 [12]) and the specimen (X5CrNi18-10 [13]). The remaining part of the alloys consist of iron (Fe).

mass percent p^M	C	Si	Mn	S	Cr	Ni	ρ_{Alloy} in g/cm³
16MnCr5	0.16	0.2	1.1	0.035	0.9	-	7.81
X5CrNi18-10	0.07	1.0	2.0	0.03	18.0	9.5	7.90

The underlying calculations shown in Eq. (3) [14] determine the absorption coefficient $\mu(E)$ for a certain energy E by adding up the weighted mass attenuation coefficients $\mu(E)\ /\ \rho$ (from the database of the national Institute of Standards and Technology NIST [15]) for each of the n elements of the alloy chemical composition in mass percent p^M (Table 1). Linear interpolation was used between the discrete sampling points of the NIST database.

$$\mu(E) = \rho_{alloy} \cdot \sum_{i=1}^{n} \left(\frac{\mu(E)}{\rho}\right)_i \cdot p_i^M \tag{3}$$

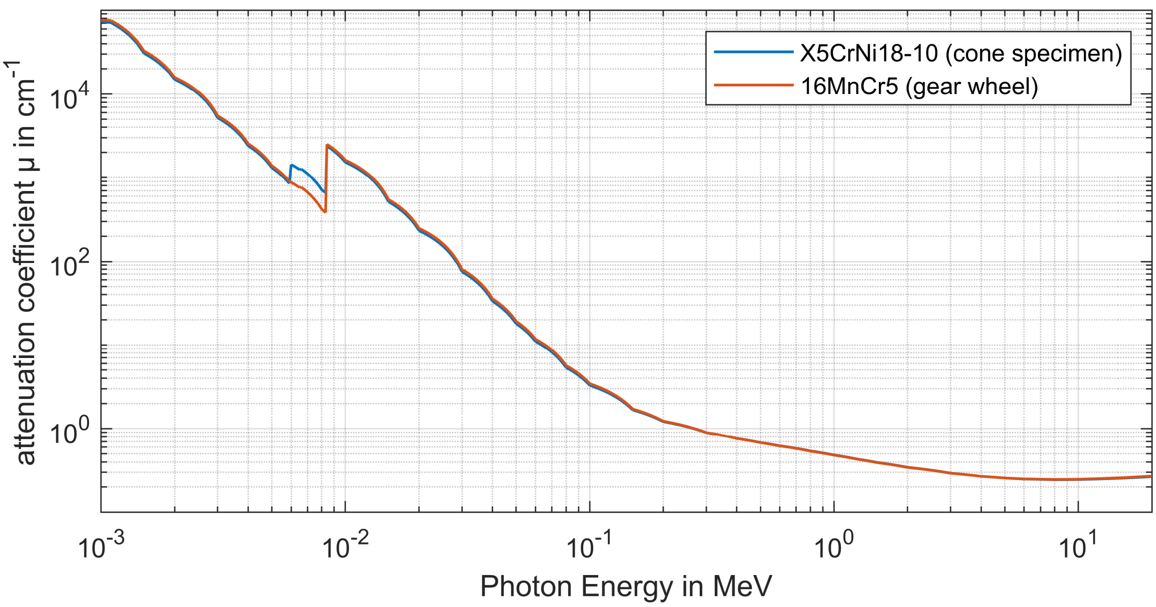

Fig. 3: Calculated absorption coefficients of the gear (16MnCr5) and the specimen (X5CrNi18-10).

2.2. Extraction of the Absorption Curve and Generation of a Correction Lookup-Table

To obtain the reference data, the object was mounted onto the rotatory stage of the CT and a full scan was performed. The settings regarding the X-ray tube and the detector were chosen to match those of the gear measurement. After the tomographic reconstruction of the measurement consisting of 1500 projections, a geometric regression analysis with a cone model ("cone fit") was performed onto the segmented volume data. Both steps (surface determination and cone fit) were carried out using VGS. Now, a full 3-D model of the CT scan can be set up in an arbitrary coordinate system (we used the Siemens CERA 3.0.3 world coordinate system (WCS), as described in [11]). The cone model can then be placed into the scene by using the geometric parameters of the regression analysis (Fig. 4).

The generation of the 3-D scene makes it possible to apply a ray tracing routine in order to determine the cone penetration lengths associated with each detector pixel. For that, the connection vectors for each pixel to the X-ray source were tested against the analytical cone model, determined by the VGS fit, using the intersection test described in [16]. The usage of the analytical description of the cone was used mainly for performance reasons, as this approach was significantly less computationally demanding than using the triangulated model resulting from the surface determination. This can be justified, because the turned part was manufactured very accurately. The correlation of the value of each pixel and the calculated penetration lengths then formed the desired relationship between intensity attenuation and penetration length. This approach was then repeated for each of the 1500 projections, thus laying the foundation for a statistically very robust absorption model. At this point, the absorption model consisted of more than 10^9 grid points.

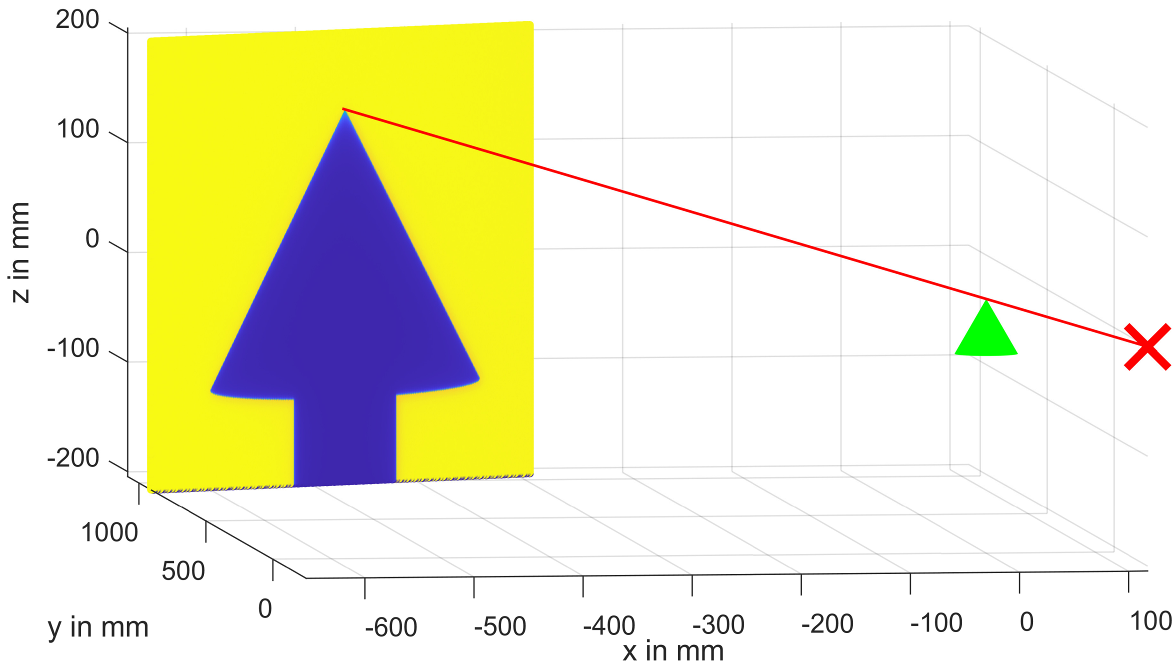

Fig. 4: Geometric setup for the intersection setup with X-ray source (red cross), the measured cone geometry (green cone) and the corresponding projection (RGB colour map for better visualization). The red line connects source with the cone tip up to the detector, the figure is true to scale.

In order to build a usable lookup table, which could then be used to correct the projections of the gear measurement, several data processing steps needed to be performed. First, the model was reduced to data points, which were located inside a target cone half angle of 1°. This excludes the faulty influence of the cone curvature onto the calculated grid points, which increases rapidly with decreasing intersection angle between the test ray and the cone shell surface. Secondly, all model grid points, which exhibited a cone penetration length of smaller than 250 µm were excluded from the model. This was done because of the limited detector pitch and because the model showed degenerative behaviour for penetration lengths below that point. These two measures reduced the number of model points to $3.1 \cdot 10^7$. Lastly, the model points needed to be binned in order to acquire unique x/y grid points to increase the subsequent regression analysis. The absorption values are represented by discrete values in the 16 bit value range, but for each of those values there possibly existed more than one penetration length. Thus, a unique penetration length for each discrete absorption value was calculated by the mean value of those distances within less than three scaled median absolute deviations from the median of those distances [17].

Following the data binning, the logarithms $-\log I/I_0$ of the grey values were taken ($I_0 = 2^{16} - 1$) and the absorption model was finalized by piecewise defined polynomial regression analyses. This was mainly done because of the requirement that the model must include the data point (0/0), which represents the maximum intensity on the logarithmic scale at zero X-ray penetration length, as shown in Fig. 5. Because of that condition on the solution of polynomial regression analysis, the solution of a constrained linear least-squares problem in the form of Eq. (4) was necessary [18].

$$\min_x \frac{1}{2} \|C \cdot x - d\|_2^2 \text{ such that } A_{eq} \cdot x = b_{eq} \tag{4}$$

Here, C represents the Vandermonde matrix, up the desired degree n of the polynomial regression model in Eq. (5). The variables x and d represent the value pairs of the binned absorption curve. The linear equality constraint of (0/0) is realized by the definition of A_{eq} and b_{eq}, as shown exemplarily in Eq. (5). Here, the superscript index 1 stands for model part 1, which requires the equality constraint (0/0).

$$C(x_1, x_2, \dots, x_n) = \begin{pmatrix} x_1^{n-1} & \cdots & x_1^1 & x_1^0 \\ x_2^{n-1} & \cdots & x_2^1 & x_2^0 \\ \vdots & \ddots & \vdots & \vdots \\ x_n^{n-1} & \cdots & x_n^1 & x_n^0 \end{pmatrix} \tag{5}$$
$$A_{eq}^1 = (0^{n-1} \quad \cdots \quad 0^1 \quad 0^0),\ b_{eq}^1 = 0$$

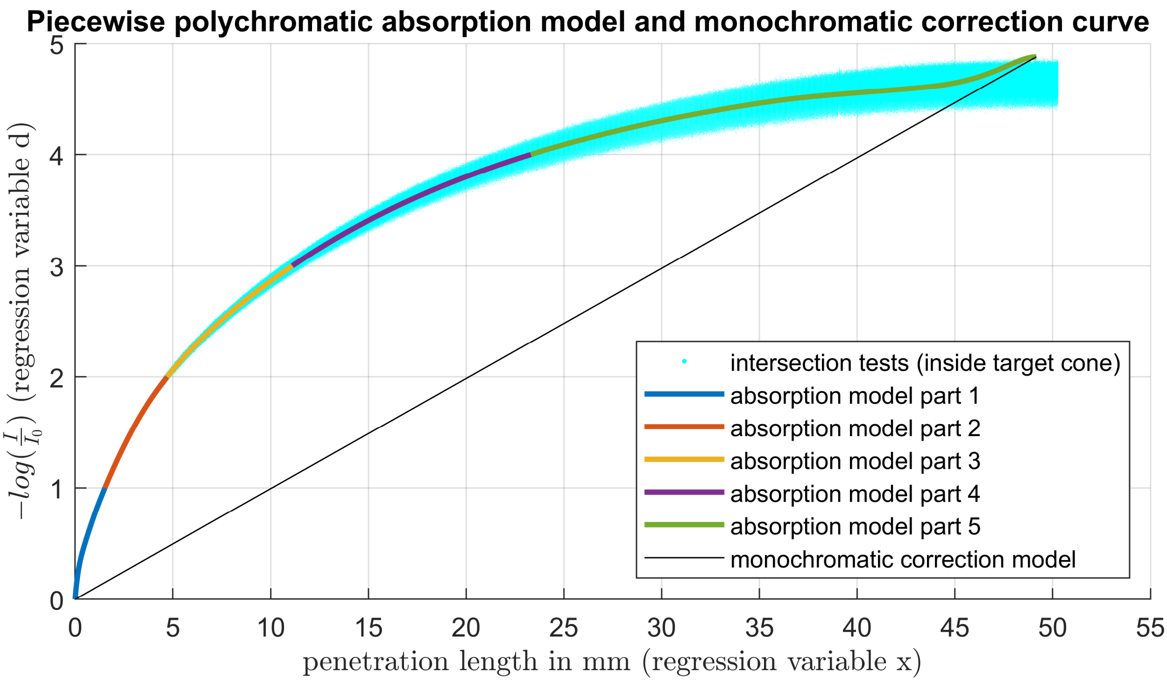

Fig. 5: Absorption model represented by piecewise defined polynomial functions with C^0 continuity based on the binned intersection test data satisfying the target cone half angle condition of 1°and a minimum penetration length of 250 µm. Material X5CrNi18-10; X-ray tube settings 225 kV, 200 µA.

For numerical robustness, the regression was performed piecewise, with subsequent polynomials satisfying C^0 continuity. Thus, the constraint $A_{eq} \cdot x = b_{eq}$ for the following curve satisfies the last point of the previous curve. Fig. 5 shows the final regression results. Finally, all required features to create a correction lookup table were prepared. The correction for a projection value is dependent on the definition of a monochromatic correction curve (Fig. 5). That means, that the corrected value of a pixel value is determined by the value of the monochromatic correction model for the same penetration length, which is defined by the absorption model. After the correction of all projections, the tomographic reconstruction was performed again, using Siemens CERA XPlorer 3.0.3 and the same settings as for the previous reconstruction.
All data processing steps but the correction of the projection itself, can be pre-computed, which reduces the actual required data processing steps for the correction of any measurement to the highly performant application of lookup table operations. The operations required for the application of a 16 bit lookup table are basically only limited to the I/O speed of the used data connection.

3. Results

The correction of the grey values resulted in a visible reduction of beam hardening artefacts (Fig. 6, left), in comparison to the uncorrected data (Fig. 1). Nonetheless, the image exhibits a high noise level, which prevented a successful surface determination. Because of that, the projections were subject to an additional Gaussian filtering (MATLAB, sigma = 5 pixel) after the application of the BHC. This operation resulted in an increased contrast in the volume data between the measurement object and the background (Fig. 6, right).

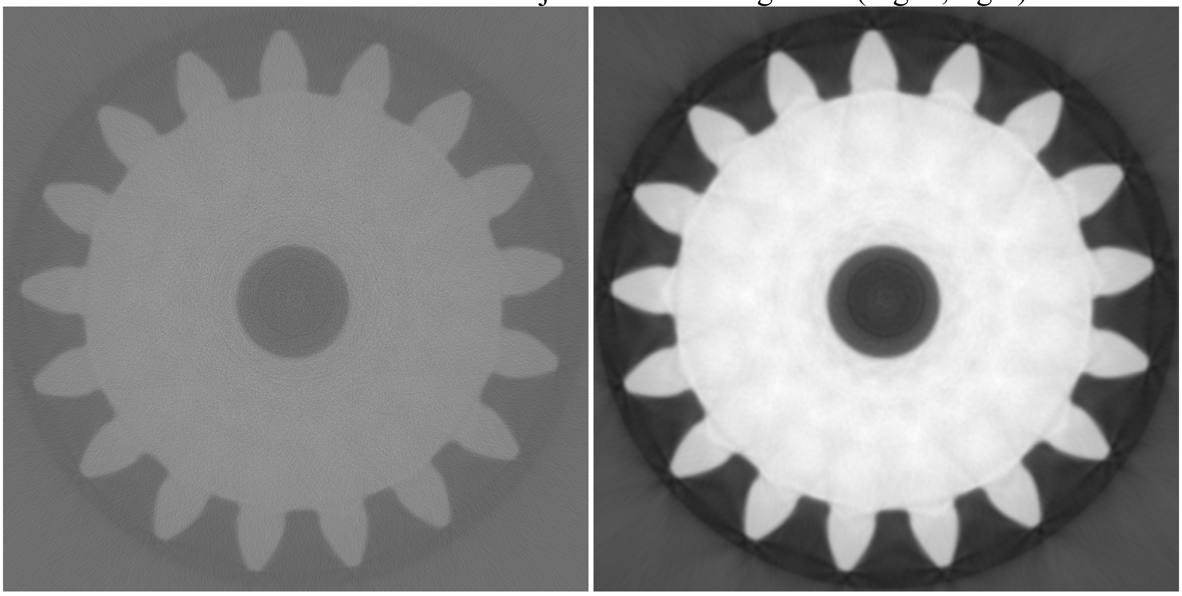

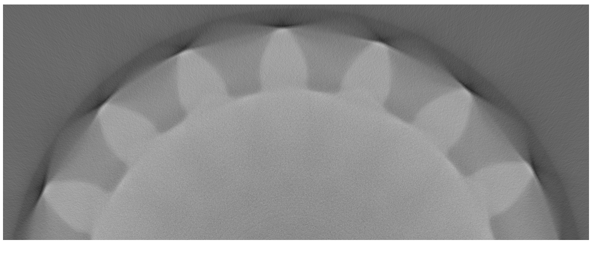

Fig. 6: Visualization of a volume slice (z = 630 voxel) of the corrected measurement utilizing the proposed method (left). Correction result (right, same slice) with an additional gauss filter (sigma = 5 pixel) of the projections after correction. The colour maps contain the 16 bit value range resulting after reconstruction. The small image (right) shows the unaltered top part of the same slice of the original measurement from Fig. 1.

The surface determination of the reconstructed volume of the post-filtrated projections (Fig. 6, right) lead to satisfying results when creating a nominal-actual comparison against the CAD model of the gear wheel (Fig. 7). The absolute deviations in the middle part of the tooth flanks do not exceed 15 µm. Note that due to the lack of a reference measurement, it is impossible to distinguish between geometric work piece deviations and measurement errors. Similar results, which means slightly noisier but also more accurate with respect to the CAD model, could be achieved by filtering of the volume data (according to Fig. 6, left; filtering result not shown) using a Gaussian filter of size 15 in VGS, followed by the surface determination and nominal-actual comparison (Fig. 8).

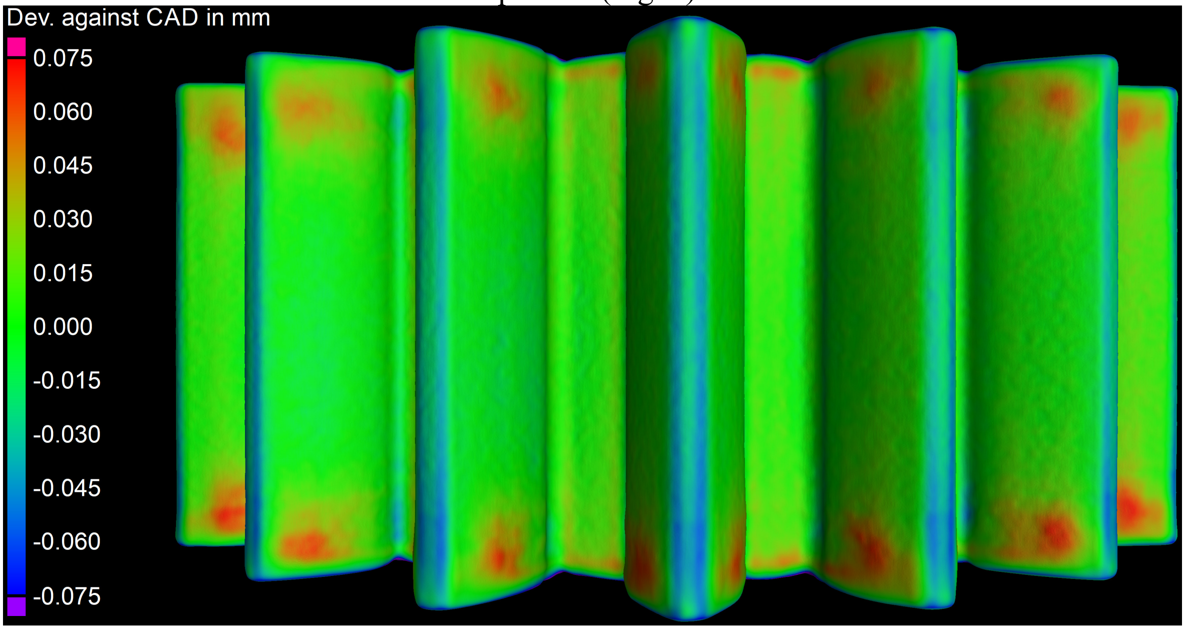

Fig. 7: Nominal-actual comparison of the reconstructed volume using the post-filtered projections (Fig. 6, right) against the nominal CAD model.

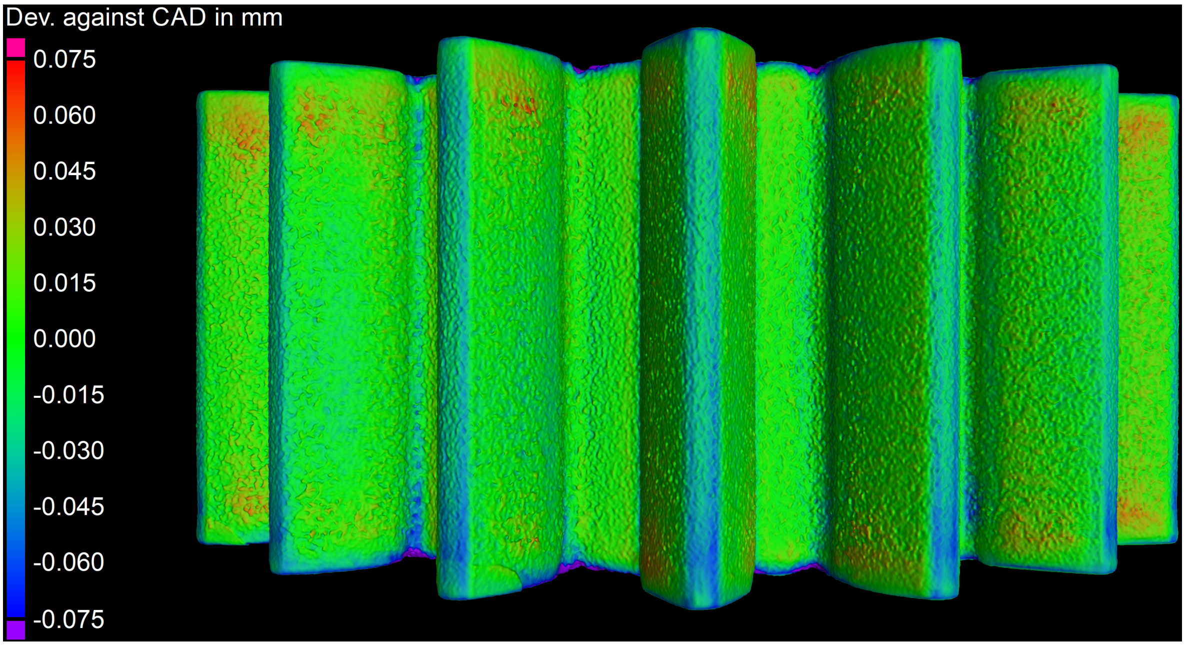

Fig. 8: Nominal-actual comparison of the reconstructed volume against the nominal CAD model using the BHC corrected projections (Fig. 6, left), followed by a volume data Gaussian filter (size = 15).

4. Discussion

We could show, that it was possible to significantly improve the CT volume data quality by estimating the faulty influence of X-ray beam hardening onto the measurement result. After the correction, surface determination was possible and a nominal-actual comparison with the CAD model could be calculated. This was not possible without the correction method. The investigation showed, that the problem of beam hardening is closely related to a low signal-to-noise ratio (SNR) of the reconstructed volume data, which can also impair a successful surface determination. In this contribution, we did not take into account the effect of X-ray scattering, which has a comparatively high influence for scenarios with low SNR. We are aware of the fact, that our calculated absorption model (Fig. 5) is also corrupted by X-ray scatter effects, which are inherently different for the gear wheel measurement. Nonetheless, this effect on the volume data could successfully be reduced by the introduction of an additional Gaussian filter onto the corrected projections (Fig. 7) and the volume data (Fig. 8), which lead to satisfying results.

5. Summary and outlook

The implementation of the beam hardening correction method discussed in this paper focused on a robust and easy to implement procedure, which can be utilized for any industrial CT. The determination of the absorption curve for a specific material was carried out exploiting a standard CT measurement of a cone-shaped specimen, which does not require any additional operating states of the CT system. From that point on, the data processing pipeline is straightforward and easy to implement for the specific use case. The quality of the results can further be increased by Gaussian filtering of the corrected projections or the reconstructed volume.

Future examinations will focus on examining the portability of the procedure on other measurement tasks, as well as on other materials, such as aluminium. Additionally, the validity of the introduced filtering operations regarding the measurement uncertainty must be proven, in order to be used by default within the data processing pipeline.

Acknowledgments

The authors would like to thank the German Research Foundation (DFG) for supporting the research project “FOR 2271 process-oriented tolerance management based on virtual computer-aided engineering tools” under grant number HA 5915/9-1 and for the financial support of the acquisition of the CT system "Zeiss Metrotom 1500" through Grant No. 324672600. The authors thank the Institute of Manufacturing Technology (LFT, FAU Erlangen-Nürnberg) for providing the steel gear wheel used for demonstration purposes in this article.

References

[1] L. A. Feldkamp, L. C. Davis, and J. W. Kress, “Practical cone-beam algorithm,” *Journal of the Optical Society of America A: Optics and Image Science, and Vision*, vol. 1, no. 6, pp. 612–619, 1984.

[2] S. Kasperl, “Qualitätsverbesserungen durch referenzfreie Artefaktreduzierung und Oberflächennormierung in der industriellen 3D-Computertomographie,” Dissertation, Friedrich-Alexander-Universität Erlangen-Nürnberg (FAU), 2005.

[3] F. E. Boas and D. Fleischmann, “CT artifacts: causes and reduction techniques,” *Imaging in Medicine*, vol. 4, no. 2, pp. 229–240, 2012.
[4] M. Kachelrieß, “Reduktion von Metallartefakten in der Röntgen-Computer-Tomographie,” Dissertation, Friedrich-Alexander-Universität Erlangen-Nürnberg (FAU), Erlangen, 1998.
[5] A. C. Kak and M. Slaney, *Principles of computerized tomographic imaging*. New York: IEEE Press, 1988.
[6] R. E. Alvarez and A. Macovski, “Energy-selective reconstructions in X-ray computerised tomography,” *Phys. Med. Biol.*, vol. 21, no. 5, pp. 733–744, 1976.
[7] L. Gjesteby *et al.,* “Metal Artifact Reduction in CT: Where Are We After Four Decades?,” *IEEE Access*, vol. 4, pp. 5826–5849, 2016.
[8] M. Katsura, J. Sato, M. Akahane, A. Kunimatsu, and O. Abe, “Current and Novel Techniques for Metal Artifact Reduction at CT: Practical Guide for Radiologists,” (eng), *Radiographics : a review publication of the Radiological Society of North America, Inc*, vol. 38, no. 2, pp. 450–461, 2018.
[9] G. T. Herman, “Correction for beam hardening in computed tomography,” *Phys. Med. Biol.*, vol. 24, no. 1, pp. 81–106, 1979.
[10] L. A. Shepp and B. F. Logan, “The Fourier reconstruction of a head section,” *IEEE Trans. Nucl. Sci.*, vol. 21, no. 3, pp. 21–43, 1974.
[11] Siemens Healthcare GmbH, *CERA: User Manual (Part 1 – CERA API).* Version 3.0, 2015.
[12] STAUBER GmbH Metalltechnologie, *1.7131 - Werkstoff 1.7131 Datenblatt.* [Online] Available: https://www.stauberstahl.com/werkstoffe/17131-werkstoff-datenblatt/. Accessed on: May 31 2019.
[13] STAUBER GmbH Metalltechnologie, *1.4301 - Werkstoff 1.4301 Datenblatt.* [Online] Available: https://www.stauberstahl.com/werkstoffe/14301-werkstoff-datenblatt/. Accessed on: May 31 2019.
[14] C. Niggemann, *Wissensbasiertes System zur Verbesserung dimensioneller Messungen mittels Röntgen-Computertomografie,* 1st ed. Aachen: Apprimus-Verl., 2012.
[15] NIST - International Institute of Standards and Technology - U.S. Department of Commerce, *X-Ray Mass Attenuation Coefficients.* [Online] Available: https://physics.nist.gov/PhysRefData/XrayMassCoef/tab3.html. Accessed on: May 31 2019.
[16] D. Eberly, *Geometric Tools: Intersection of a Line and a Cone.* [Online] Available: https://www.geometrictools.com/Documentation/IntersectionLineCone.pdf. Accessed on: May 31 2019.
[17] The MathWorks, Inc., *rmoutliers: Detect and remove outliers in data.* [Online] Available: https://www.mathworks.com/help/matlab/ref/rmoutliers.html. Accessed on: May 31 2019.
[18] The MathWorks, Inc., *lsqlin: Solve constrained linear least-squares problems.* [Online] Available: https://www.mathworks.com/help/optim/ug/lsqlin.html. Accessed on: May 31 2019.